Hydraulic characterization of aquifers by thermal response testing: Validation by large-scale tank and field experiments

Valentin Wagner,[1] Peter Bayer,[2] Gerhard Bisch,[3] Markus Kübert,[4] and Philipp Blum[1]

[1] Thermal response tests (TRTs) are a common field method in shallow geothermics to estimate thermal properties of the ground. During the test, a constantly heated fluid is circulated in closed tubes within a vertical borehole heat exchanger (BHE). The observed temperature development of the fluid is characteristic for the thermal properties of the ground and the BHE. We show that, when the BHE is installed in an aquifer with significant horizontal groundwater flow, this test can also be used for hydrogeological characterization of the penetrated subsurface. An evaluation method based on the moving line source equation and considering the natural occurring variability of the thermal transport parameters is presented. It is validated by application to a well-controlled, large-scale tank experiment with 9 m length, 6 m width, and 4.5 m depth, and by data interpretation from a field-scale test. The tank experiment imitates an advection-influenced TRT in a well-known layered aquifer. The field experiment was recorded with a 100 m deep BHE, installed in a gravel aquifer in southwest Germany. The evaluations of both experiments result in similar hydraulic conductivity ranges as determined by standard hydraulic investigation methods such as pumping tests and sieve analyses. Thus, advection-influenced TRTs could also potentially be used to determine integral hydraulic conductivity of the subsurface.

1. Introduction

[2] The use of temperature signals in hydrogeological field investigation has been suggested for decades [e.g., *Stallman*, 1963; *Bravo et al.*, 2002], and has recently gained significant attention, especially in the context of surface-groundwater interaction [*Cardenas*, 2010; *Lautz*, 2010]. *Anderson* [2005] and *Saar* [2011] emphasized the often unexplored potential of using natural temperature variations as a cheap, expressive, and complementary means to support hydraulic characterization of groundwater flow conditions, water balancing, and modeling on local and basin scale. So far, less interest has been on application of artificial thermal signals, which are actively induced in field measurement campaigns. Reasons for this are that standard applications and interpretation procedures do not exist, that established alternative hydrogeological investigation methods coexist, and that generation of substantial and far reaching thermal signals is challenging, time consuming, and potentially costly.

[3] In most studies with artificial heat perturbation, understanding coupled hydraulic-thermal processes is of particular interest. Evolution of thermal anomalies from injection of hot or cold water is mainly studied in the context of geothermal energy use of shallow aquifers [*Parr et al.*, 1983; *Palmer et al.*, 1992]. Thermal monitoring downgradient or in the vicinity of an artificial heat source has been gaining attention for active thermal tracer testing. *Hurtig et al.* [1994] initiated the use of distributed thermal sensors (DTS) at the Grimsel test site in Switzerland. Hot and cold water was injected in the crystalline hard rock to successfully identify fractures by thermal fluid logging. *Ma et al.* [2012] demonstrated that additional information can be exploited from combining Bromide tracer with hot water at the Hanford site, Washington. Both tracers could be used for the calibration of a groundwater and heat transport model, but density effects and intra borehole flow were identified as critical factors for the interpretation of vertical temperature variations [see also *Klepikova et al.*, 2011].

[4] In contrast to this "open test design," where mass and heat is exchanged with the subsurface, there are experiments that employ temperature signals from hydraulically closed devices without water exchange between device and soil or aquifer. *Byrne et al.* [1967] were among the first to use conductive heating devices to characterize soil water flux. In their application, a solid cylinder shelters the heater and the temperature sensors, but it significantly distorts the flow field. More recently developed devices measure thermal perturbations from a central wire, and these can be

[1]Karlsruhe Institute of Technology (KIT), Institute for Applied Geosciences, Karlsruhe, Germany.
[2]ETH Zurich, Geological Institute, Zurich, Switzerland.
[3]University of Stuttgart, Institute for Modeling Hydraulic and Environmental Systems, Stuttgart, Germany.
[4]Tewag Technologie-Erdwärmeanlagen-Umweltschutz GmbH, Starzach-Felldorf, Germany.

Corresponding author: V. Wagner, Karlsruhe Institute of Technology, Institute for Applied Geosciences, Kaiserstraße 12, Karlsruhe DE-76131, Germany. (valentin.wagner@kit.edu)

classified by the specific sensor arrangement. There are one-dimensional (1-D) [e.g., *Ochsner et al.*, 2005; *Gao et al.*, 2006], two-dimensional (2-D) [e.g., *Greswell et al.*, 2009], and three-dimensional (3-D) configurations [e.g., *Angermann et al.*, 2012]. In these studies, analytical solutions were employed to determine water flux, except of *Hopmans et al.* [2002], who applied the numerical HYDRUS-2D model for the analysis. *Ochsner et al.* [2005] emphasized that a systematical misfit between recorded and modeled data exists, which can be overcome by introducing a correction term that mitigates the advection component. *Gao et al.* [2006] explained this misfit by wall flow effects caused by the sensor.

[5] "Closed" thermal perturbation, common in hydrogeology and soil science, is confined to miniature field investigation techniques such as heat perturbation flowmeter or heat pulse sensor [*Greswell et al.*, 2009; *Angermann et al.*, 2012]. A related method for investigating ground thermal parameters, the thermal response test (TRT), is established in larger-scale geothermal applications. Typically, vertical boreholes of about 50–200 m are drilled, equipped with one or two U-tubes, and a heat carrier fluid is circulated to facilitate energy transfer between subsurface and an aboveground heat pump or resistance heater. The borehole-tubes installation is also termed borehole heat exchanger (BHE). During the TRT, the temporal development of the artificially heated fluid over a period of one or more days is analyzed. The recorded temperatures are used to calibrate analytical or numerical models to obtain the BHE-specific borehole resistance, and the thermal conductivity of the ambient ground [e.g., *Gehlin*, 2002]. Commonly, advective heat transport in penetrated aquifers is ignored. If aquifers are present then it is accounted for by introducing an effective thermal conductivity that is typically larger than the actual one describing conduction only [e.g. *Witte*, 2001].

[6] The influence of groundwater flow on TRTs has been examined in experimental and theoretical studies. To quantify the influence experimentally, two different strategies were presented. The first one compares a groundwater-influenced TRT to one conducted in comparable geology [e.g., *Chiasson and O'Connell*, 2011]. Alternatively, a forced gradient (e.g., by groundwater extraction) TRT is contrasted with results from undisturbed conditions [*Witte*, 2001]. The influence of groundwater flow on the TRT result is also analyzed by numerically generated data sets [e.g., *Signorelli et al.*, 2007; *Raymond et al.*, 2011; *Wagner et al.*, 2012a; *Sharqawy et al.*, 2013]. Fitting the analytical line source model [e.g., *Mogensen*, 1983; *Signorelli et al.*, 2007], or the cylinder source model [*Gehlin*, 2002] is most common for TRT evaluation. Apart from these analytical models, there are numerical 1-D [e.g., *Gehlin*, 2002], 2-D [*Witte et al.*, 2002], and 3-D models [e.g., *Signorelli et al.*, 2007; *Raymond et al.*, 2011] applied for more detailed TRT analysis. However, many of these standard analytical models (i.e., line and cylinder source models) neglect advective heat transport in the ground. To overcome this limitation, *Chiasson and O'Connell* [2011] and *Wagner et al.* [2013] suggested a conduction and advection sensitive model calibration approach for the TRT analysis. In *Wagner et al.* [2013], we revealed that there is a systematical misfit between actual and estimated Darcy velocities.

Comparable to the approach by *Ochsner et al.* [2005] and *Gao et al.* [2006] for heat injection devices, a correction term is introduced.

[7] The main objective of the current study is to determine the integral hydraulic conductivity of an aquifer by thermal response testing. The study builds up on the theoretical analysis presented in *Wagner et al.* [2013]. We introduce the TRT evaluation as a method to characterize exclusively the groundwater flow regime, and validate the evaluation procedure in laboratory and field applications. This changes the motivation of standard TRT application, which is mainly focused on thermal parameters, such as thermal conductivity and thermal borehole resistance, describing heat conduction from heated BHE. We recognize, in line with the results by the study of *Ma et al.* [2012] on "open" thermal tracer testing, that thermal conduction and dispersion are much less sensitive than hydraulic parameters (i.e., hydraulic conductivity) for advection-influenced systems. In the following, moderate value ranges of thermal parameters to describe heat transport in aquifers are discussed. First, the technical principles of TRT are briefly explained. Second, the moving line source-based TRT interpretation to determine the vertically integrated Darcy velocity of an aquifer is introduced. By applying Darcy's law, an integral aquifer hydraulic conductivity value is estimated. Then comprehensive large-scale tank and field experiments are described, one at a laboratory in Stuttgart and one at a field site in the town of Schwanau, Germany. These are used for validation. Finally, we discuss the applicability of the developed method, and conclude upon its robustness and potentials for improvements.

2. Methodology

2.1. Technological and Theoretical Background

[8] Closed geothermal systems are frequent applications for low-enthalpy thermal energy provision. In Europe alone, there are currently far more than one million reported installations [*Bayer et al.*, 2012]. The technological principle is straightforward: in the tubes of one or multiple adjacent boreholes a heat carrier fluid is circulated to establish a temperature gradient between borehole and ground. This stimulates conductive heat transport from or toward the borehole heat exchanger (BHE). In the closed tubes, the heat carrier fluid transports heat or cold to an aboveground receptor, such as a heat pump that supplies the heating demand of buildings. For cooling, only a circulating pump or a reversible heat pump is used. The TRT is an established field experiment to support design of closed geothermal systems [*Gehlin*, 2002; *Signorelli et al.*, 2007; *Sharqawy et al.*, 2009b]. It is employed, usually in the planning or pilot phase, to gain insights into the heat transport characteristics of the ground and of the transition between ground and heat carrier fluid. The better the geothermal system can extract heat (or cold) from the ground, the smaller the required length of the borehole and the lower the installation costs [*Blum et al.*, 2011].

[9] During the TRT, the heat carrier fluid is warmed up at the inlet of the borehole tube(s) and circulated for one or more days. By recording the temperature at the outlet, the heat loss to the ground is monitored. Assuming only
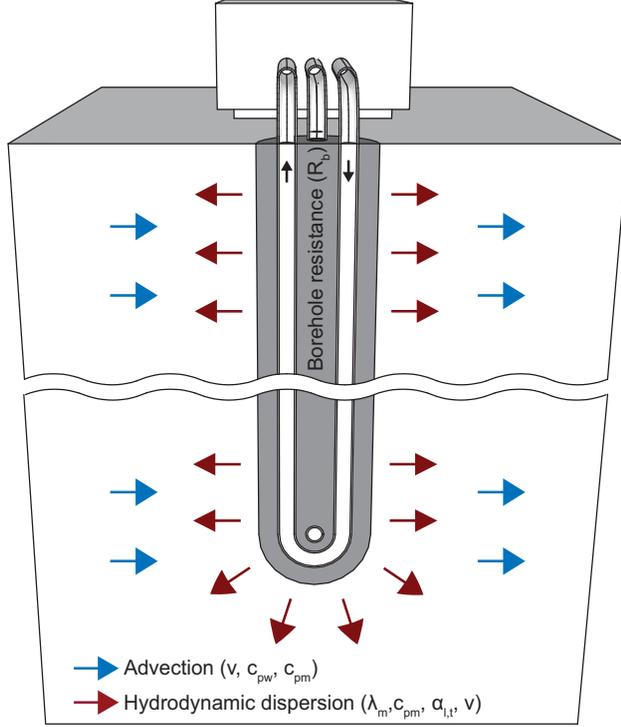
Figure 1. Borehole heat exchanger (BHE) during a thermal response test (TRT) with heat transfer processes and parameters accounted for by the moving line source (equation (6)) (thermal borehole resistance R_b; Darcy velocity v; thermal conductivity of the porous media λ_m; volumetric heat capacity of the porous media c_{pm}; volumetric heat capacity of the groundwater c_{pw}; longitudinal and transversal dispersivity α_l and α_t).

conductive heat loss and integrating over the entire borehole length, the Kelvin line source theory is typically applied [e.g., *Carslaw and Jaeger*, 1959]. The analytical line source equation describes conductive heat transport from the borehole to the ground that is simulated as an infinitely small linear structure. In practice, a logarithmic approximation of the Kelvin line source theory is often used for the calibration by straight line fitting on semilog scale to the temperature time series recorded during the TRT. This procedure is comparable to pumping test interpretation in hydrogeology.

[10] The TRT is conducted to typically estimate the values of two thermal parameters such as the mean effective thermal conductivity of the ground and the thermal borehole resistance. According to Fourier's law, the thermal conductivity governs the conductive heat flux from or toward the borehole for a given temperature gradient. In many applications, the tubes are embedded in bentonite grout [*Wagner et al.*, 2013]. Detailed simulation of the transport processes between borehole wall and carrier fluid in the tubes requires advanced numerical models, which simulate the discrete parts of a BHE. Instead of this, in the analytical line source-based simulation, the thermal borehole resistance R_b is introduced serving as the bulk parameter to quantify the thermal effects inside the BHE (Figure 1).

[11] If BHEs operate in aquifers, advection commonly improves heat transfer and system efficiency. Since hydrogeological insight is often lacking, this process is not further examined and opportunities are lost for more economic (shorter) boreholes [e.g., *Blum et al.*, 2011]. Thus, recently, attention has grown toward the role of groundwater flow, and the additional advective heat transport component that balances thermal anomalies evolving around such BHEs. There are analytical [e.g., *Chiasson and O'Connell*, 2011; *Molina-Giraldo et al.*, 2011b] and numerical [e.g., *Signorelli et al.*, 2007; *Hecht-Méndez et al.*, 2010; *Raymond et al.*, 2011] studies, which analyze the effects of simultaneous heat advection and hydrodynamic heat dispersion (Figure 1). To be able to distinguish advective and conductive components in a groundwater-influenced TRT, *Chiasson and O'Connell* [2011] and *Wagner et al.* [2013] suggest using the infinite moving line source model. The infinite moving line source equation approximates the BHE as an infinite line shape heat source (or sink) with a constant heat flux. The time-dependent temperature variation in the ground caused by the heat source is given by [*Carslaw and Jaeger*, 1959]

$$T_{sub}(x,y,t) - T_0 = \frac{q}{4\pi c_{pm}\sqrt{D_l D_t}} \exp\left[\frac{v_{th}x}{2D_l}\right]$$

$$\int_0^{\frac{v_{th}^2 t}{4D_l}} \exp\left[-\left(\frac{x^2}{D_l} + \frac{y^2}{D_t}\right)\frac{v_{th}^2}{16D_l u} - u\right]\frac{du}{u} \quad (1)$$

[12] In this study, T represents the temperature (°C), x and y are the Cartesian coordinates (m) with the BHE at the origin, t is the time (s), q is the heat injection per unit length (W m^{-1}), c_{pm} is the volumetric heat capacity of the porous media (J m^{-3} K^{-1}), and u is the integration variable. Temperature T_0 describes the undisturbed conditions at the initial state.

[13] Equation (1) describes conductive and advective heat propagation in homogeneous porous media. The effective heat transport velocity is defined as

$$v_{th} = v\frac{c_{pw}}{c_{pm}} \quad (2)$$

where v is the Darcy velocity (m s^{-1}) and c_{pw} the volumetric heat capacity of the groundwater (J m^{-3} K^{-1}). Subscript th denotes that the transport velocity (v_{th}) is thermally retarded. The effective thermal dispersion coefficients D (m s^{-2}) are in longitudinal direction

$$D_l = \frac{\lambda_m}{c_{pm}} + \alpha_l v_{th} \quad (3a)$$

and in transversal direction

$$D_t = \frac{\lambda_m}{c_{pm}} + \alpha_t v_{th} \quad (3b)$$

[14] The thermal conductivity of the porous media is λ_m (W m^{-1} K^{-1}); α_l and α_t (m) represent the longitudinal and transversal dispersivities. For TRT interpretation, the

3

temperature change of the ambient ground is calculated based on equation (1). The temperature difference inside the BHE is accounted for by the thermal borehole resistance R_b (m K W^{-1}), which is calculated as

$$R_b = \frac{T_f - T_{bw}}{q} \qquad (4)$$

[15] Temperature T_{bw} refers to the borehole wall and T_f to the heat carrier fluid. R_b relates the borehole wall temperature to the heat carrier fluid temperature [*Sutton et al.*, 2002]

$$T_f(x,y,t) = \frac{q}{4\pi c_{pm}\sqrt{D_l D_t}} \exp\left[\frac{v_{th}x}{2D_l}\right]$$

$$\int_0^{\frac{v_{th}^2 t}{4D_l}} \exp\left[-\left(\frac{x^2}{D_l}+\frac{y^2}{D_t}\right)\frac{v_{th}^2}{16D_l u}-u\right]\frac{du}{u}+T_0+R_b q \qquad (5)$$

[16] If the physical properties of the ground can be approximated as temperature independent, superposition can be applied to equation (5). Temporal superposition is used to consider multiple loads during the TRT, and consequently, to facilitate a stepwise TRT evaluation. Spatial superposition is employed to account for locally variable effects of groundwater flow. During heating, advective heat transport causes an asymmetric borehole wall temperature with lower values at the upstream. This is resolved by multiple (here, six) superimposed line sources equally positioned at the borehole wall at (x_j, y_j), which share the total heat injection rate of the TRT. Temporally and spatially superimposed equation (5) reads

$$T_f(t) = \sum_{i=1}^{m}\sum_{j=1}^{n}\frac{\frac{1}{n}(q_i - q_{i-1})}{4\pi c_{pm}\sqrt{D_l D_t}}\exp\left[\frac{v_{th}x_j}{2D_l}\right]$$

$$\int_0^{\frac{v_{th}^2(t_m - t_i)}{4D_l}} \exp\left[-\left(\frac{x_j^2}{D_l}+\frac{y_j^2}{D_t}\right)\frac{v_{th}^2}{16D_l u}-u\right]\frac{du}{u}+T_0+R_b\frac{q_i}{n} \qquad (6)$$

where m denotes the number of time steps and n the number of heat sources. At time step i, a total heat injection rate of q_i is applied to the BHE, with $t_0 = 0$ and $q_0 = 0$.

[17] By formulating the moving line source equation in dimensionless form, one is able to obtain a set of universal thermal response curves. The dimensionless coordinates are obtained by referring to the BHE length H; in x-direction: $x' = x\,H^{-1}$ and in y-direction $y' = y\,H^{-1}$. The dimensionless heat injection rate per unit length q' is formulated in the same manner, $q' = q\,q_{ref}^{-1}$. In line with the work of *Molina-Giraldo et al.* [2011b], a dimensionless temperature rise Θ is defined based on the temperature change ΔT: $\Theta = \Delta T\,c_{pm}\,D_l\,4\,\pi\,q_{ref}^{-1}$. Furthermore, the Fourier number $Fo = D_l\,t\,H^{-2}$, the Peclet number $Pe = v_{th}\,H\,D_l^{-1}$ and the effective thermal dispersion ratio $\beta = D_l\,D_t^{-1}$ are defined. Based on these dimensionless parameters, equation (6) can be expressed in dimensionless form:

$$\Theta(q',x',y',\beta,Pe,Fo) = \sum_{i=1}^{m}\sum_{j=1}^{n}\frac{1}{n}(q_i' - q'_{i-1})\sqrt{\beta}\exp\left[\frac{Pex'}{2}\right]$$

$$\int_0^{\frac{Pe^2 Fo}{4}}\exp\left[-\left(x_j'^2+\beta y_j'^2\right)\frac{Pe^2}{16u}-u\right]\frac{du}{u} \qquad (7)$$

[18] In contrast to the approach by *Chiasson and O'Connell* [2011], *Wagner et al.* [2013] also considers the hydraulic effects of the grouting material inside the borehole on the estimated parameters. *Wagner et al.* [2013] built up a two-dimensional (2-D) finite element model of a BHE in FEFLOW 5.4 [*Diersch*, 2009]. By using a fully discretized BHE, this numerical model considers the complex heat propagation inside the BHE between the heat carrier fluid, pipe wall, and the grout material, as well as advective and conductive heat transport in the surrounding ground. By comparing this high-resolution numerical model and equation (6), it was demonstrated that there is a systematic misfit between the Darcy velocities derived from realistic numerical and approximate moving line source models. The anticipated discrepancy of the numerical and analytical thermal response curves is caused by remarkable hydraulic conductivity contrast between the grouting material of the BHE and the ambient aquifer, which reaches typically more than 3 orders of magnitude, and which is not resolved by equation (6). In comparison, thermal properties of the grouting material and the aquifer are commonly in a comparable range. *Wagner et al.* [2013] demonstrated that Darcy velocity, v, in an aquifer is underestimated by equation (6) due to disregard of the low-permeable grout, and therefore, the calibrated value reflects an effective Darcy velocity. This is comparable to the findings by *Ochsner et al.* [2005] for calibration of heat pulse models. The derived effective Darcy velocity, v_{eff}, however, may be adjusted by a numerically derived correction factor C to a corrected effective Darcy velocity v_{eff}^*, which is comparable to the aquifer Darcy velocity.

$$v \approx v_{eff}^* = \frac{v_{eff}}{C} \qquad (8)$$

[19] Appropriate values of C depend on effective thermal conductivity and effective Darcy velocity, $\lambda_{m,eff}$ and v_{eff}, as shown in Figure 2. *Wagner et al.* [2013] analyzed possible effects of R_b values ranging from 0.06 to 0.12 m K W^{-1} and heat extraction/injection rates, q, varying from -50 to 75 W m^{-1} on the discrepancy between v_{eff} and v. It was demonstrated that the obtained C values are robust and insensitive to these parameters.

2.2. Parameter Estimation Procedure

[20] A two-step parameter estimation procedure is applied to determine Darcy velocity of horizontal groundwater flow. If the hydraulic gradient is known, the hydraulic conductivity can be derived (Figure 3). Hydraulic parameters such as the hydraulic conductivity, K, vary over orders of magnitude, and therefore, natural occurring Darcy velocities are highly variable. In contrast, reasonable value ranges for thermal transport parameters in aquifers are much more constrained. Hence, here, we solely focus on
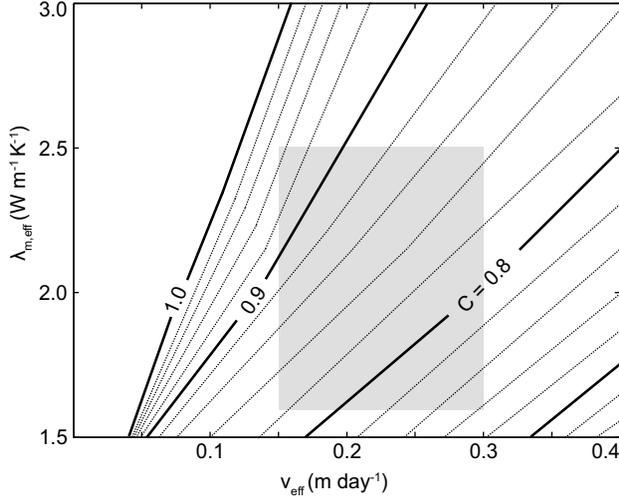
Figure 2. Values for the correction factor C depending on effective thermal conductivity, $\lambda_{m,eff}$, and effective Darcy velocity, v_{eff}. The gray area depicts the value range for the examples chosen in the present study.

was to assess the impact of thermal disturbances on the subsurface, and therefore, a detailed characterization of the hydraulic and thermal properties was performed. The volumetric heat capacity of the aquifer was $c_{pm} = 2.79 \pm 0.01$ MJ m^{-3} K^{-1} and the thermal conductivity was $\lambda = 2.42 \pm 0.28$ W m^{-1} K^{-1}. In contrast to this small range of the thermal properties, the hydraulic conductivity measured at this site varies by 3 orders of magnitude (1.8×10^{-4} m s$^{-1} \leq K \leq 1.7 \times 10^{-2}$ m s^{-1}). At the prominent Borden test site, *Macfarlane et al.* [2002] and *Sudicky* [1986], among others, described the moderate heterogeneity of the studied aquifer (1.0×10^{-5} m s$^{-1} \leq K \leq 3.1 \times 10^{-4}$ m s^{-1}). In the field experiments by *Palmer et al.* [1992], the volumetric heat capacity was specified as $c_{pm} = 2.84$ MJ m^{-3} K^{-1} and the variability of $\lambda_m = 2.1 \pm 0.3$ W m^{-1} K^{-1} was comparably small. A third exemplary study site is located 32 km north of Mobile, Alabama. *Parr et al.* [1983] characterized the confined aquifer to assess its potential for thermal energy storage, and they obtained $c_{pm} = 2.78$ MJ m^{-3} K^{-1} and $\lambda_m = 2.3 \pm 0.19$ W m^{-1} K^{-1}. A transmissivity of 1130–1140 m day^{-1} was determined by a standard pumping test. With an aquifer

the identification of effective Darcy velocity, v_{eff}, and K. The Nelder-Mead algorithm [*Nelder and Mead*, 1965; *Lagarias et al.*, 1998; *Bayer and Finkel*, 2007] is used to determine v_{eff}, by fitting equation (6) to measured temperature time series. This is achieved by minimizing the root-mean-squared error (RMSE). Further thermal transport parameters are set fixed during the fitting step. In order to examine the variability of v_{eff} depending on the thermal transport parameter settings, the v_{eff} fitting step is repeated for alternative combinations. Given ranges of λ_m, c_{pm}, α_l, and R_b are discretized and all combinations of these discretized parameter values are tested. This is exhaustive but, with an analytical model, the computational effort is moderate. Not all combinations enable satisfactory curve fitting, and a threshold for the RMSE is suggested to exclude non-plausible results. As a result, we obtain a complete set of possible v_{eff}, as well as the associated residuals from the fitting, while assuming limited knowledge on thermal transport parameters. The derived v_{eff} values are corrected by equation (8) to estimate v, and we arrive at an estimate of K with the hydraulic gradient of the aquifer. This two-step parameter estimation procedure is a straightforward method, which may be replaced by any alternative. We favor the presented steps to capture all possible values of v_{eff}. Alternatively, this may also be studied with a Bayesian or evolutionary algorithm.

[21] The more the value range of thermal parameters can be constrained, the more precisely the Darcy velocity can be determined. The thermal properties of aquifers are less variable than hydraulic properties [e.g., *Parr et al.*, 1983; *Anderson*, 2005], and by means of established empirical or statistical relationships they can be estimated at the field site [e.g., *Woodside and Messmer*, 1961; *Menberg et al.*, 2013]. Support for this can be found when comparing case studies on unconsolidated aquifers. For example, *Markle et al.* [2006] analyzed the evolution of a thermal plume in a glacial-outwash aquifer of the Tricks Creek wetland complex in southwest Ontario, Canada. Their main objective

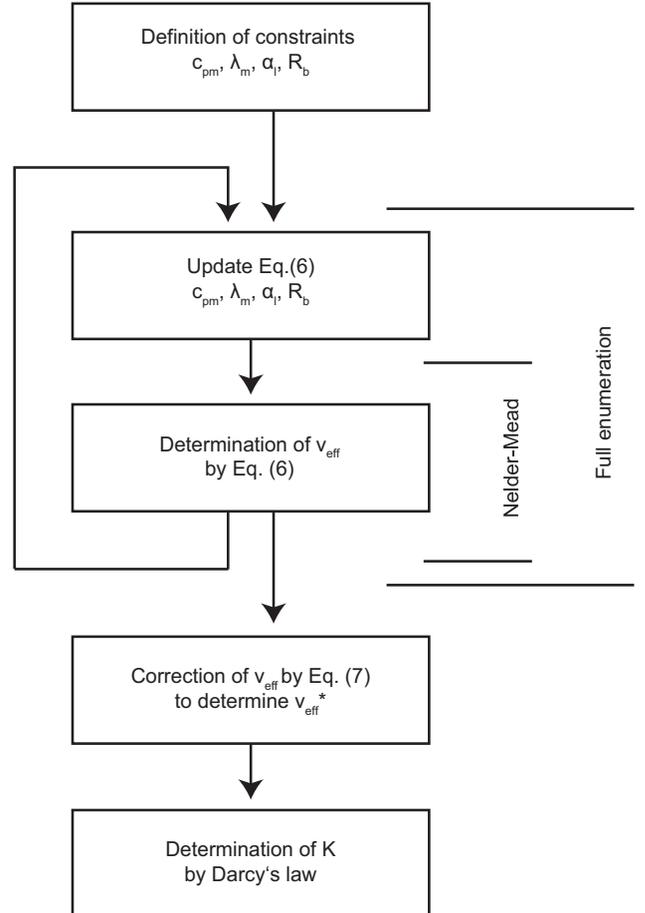**Figure 3.** Optimization schedule applied to combine a local Nelder-Mead optimization of v_{eff}, and full enumeration grid search on c_{pm}, λ_m, α_l, and R_b. Determined v_{eff} values are corrected by equation (8) and if the hydraulic gradient is known, v_{eff}^* can be transferred to an integral hydraulic conductivity (K).

thickness of about 31 m and mean hydraulic conductivity around $K = 4.2 \times 10^{-3}$ m s^{-1}.

[22] The volumetric heat capacity of porous media is commonly calculated by the arithmetic mean of the components [e.g., *Parr et al.*, 1983; *Palmer et al.*, 1992; *Markle et al.*, 2006]. For an idealized aquifer with one solid phase (i.e., mainly quartz) and one fluid phase (i.e., water), the volumetric heat capacity can be estimated by [e.g., *Rau et al.*, 2012]:

$$c_{pm} = nc_{pf} + (1-n)c_{ps} \qquad (9)$$

where c_{pf} and c_{ps} are the volumetric heat capacities of the fluid and the solid phase (note: if the fluid phase is water, c_{pf} is equal to c_{pw}). The porosity of unconsolidated materials is variable and for instance, in *Fetter* [2001], the porosity of sand and gravel mixture ranges typically from 20% to 35%, and may reach 50% in well-sorted material. This yields a span of c_{pm} as illustrated in Figure 4, which also captures those values reported above in the three case studies. Additionally, the values from the studied tank experiment (Table 1), which will subsequently serve as validation case for this study, are shown.

[23] Appropriate estimation of thermal conductivity of saturated porous media, λ_m, is more challenging, because the value does not only depend on fraction of components or phases. There are several other factors, which are also relevant, such as bulk density, shape, size, and arrangement of the grains [*Markle et al.*, 2006]. Accordingly, several methods to narrow down values of λ_m coexist. Maximum values are given by the arithmetic mean of component-specific quantities, and the harmonic mean denotes the minima [*Woodside and Messmer*, 1961]. The geometric mean describes a random distribution, which was successfully applied in a study by *Menberg et al.* [2013] validating the results of a TRT. A more specific, empirical approach is the one proposed by *de Vries* [1963]. It is particularly suited for unconsolidated soil, because it also considers the shape of the particles by the form factor g_i. For spherical particles, $g_1 = g_2 = g_3 = 1/3$,

$$\lambda_m = \frac{n\lambda_f + (1-n)\lambda_s F_1}{n + (1-n)F_1} \qquad (10)$$

$$F_1 = \frac{1}{3}\sum_{i=1}^{3}\left[1 + \left(\frac{\lambda_s}{\lambda_f} - 1\right)g_i\right]^{-1} \qquad (11)$$

where the thermal conductivity of the fluid phase is λ_f, and of the solid phase λ_s. The factor F_1 defines the average temperature gradient in the fluid and solid phase.

[24] Figure 4 b depicts obtained thermal conductivity value ranges for unconsolidated gravel/sand mixtures, assuming a two-phase system of spherical quartz grains and water. Again, this range captures the measured and reported (mean) values. Based on the findings from the exemplary measurements and the empirical relationships, values of λ_m vary within a small range, which is 2.2 ± 0.55 W m^{-1} K^{-1}. This range represents a variability of $\pm 25\%$ around the mean thermal conductivity value. This variability is even less for the heat capacity, c_{pm} with a mean of 2.79 MJ m^{-3} K^{-1}, and values that spread from 2.51 to 3.07 MJ m^{-3} K^{-1}, which is $\pm 10\%$ of the mean value. These
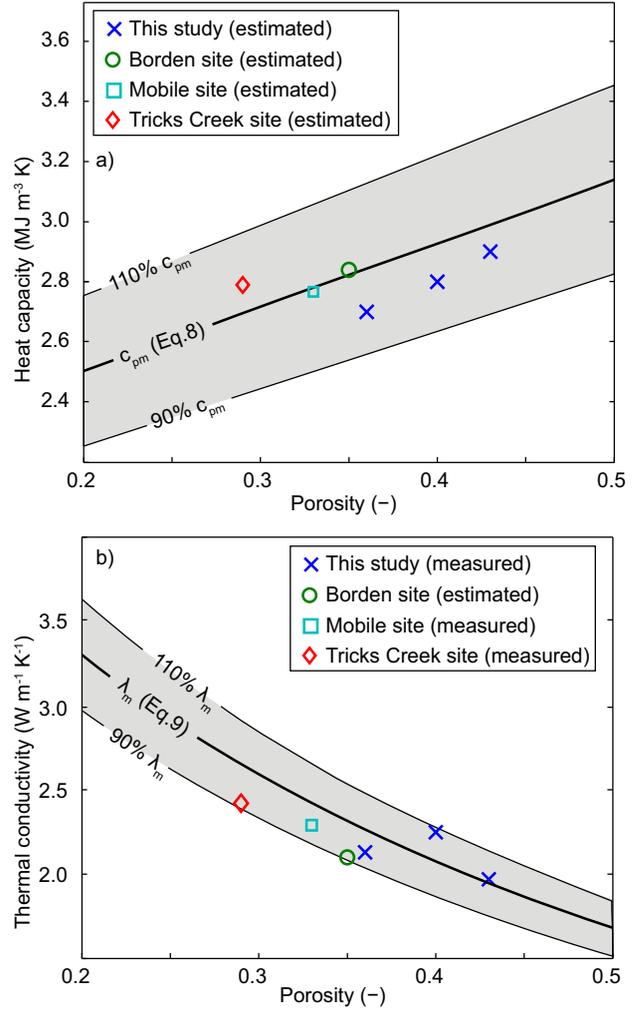

Figure 4. (a) Volumetric heat capacity values compared to estimates based on equation (9) for water/quartz system, with: $c_{pf} = 4.2$ MJ m^{-3} K^{-1} and $c_{ps} = 2.1$ MJ m^{-3} K^{-1}. (b) Thermal conductivity values compared to the range derived by equation (10). The thermal conductivity of the porous medium is calculated for a quartz solid phase with 6 W m^{-1} K^{-1}, and water as fluid phase with 0.6 W m^{-1} K^{-1}.

limits are also adopted to constrain the parameter values in this study.

[25] Differential advection leads to mechanical dispersion, which is quantified by thermal longitudinal and transversal dispersivity in equations (3a) and (3b). It is commonly assumed that transversal dispersivity is 1 order of magnitude smaller than longitudinal dispersivity [e.g., *Bear and Cheng*, 2010; *Molina-Giraldo et al.*, 2011a]. This relationship is also applied for this study. In order to account for the scale dependency of dispersion, appropriate dispersivity values are related to the field scale. *Molina-Giraldo et al.* [2011a] compiled longitudinal thermal dispersivity and corresponding field scales of previous studies. *Gelhar et al.* [1992] suggested taking the distance covered by transport during the experiment as a field scale. A rough estimate would be effective heat transport velocity times experimental duration. Until now, it is still not clear how

Table 1. Properties of the Different Sedimentary Layers in the Tank Experiment

	Middle Sand Layer		Coarse Sand Layer		Fine Sand Layer	
	Min	Max	Min	Max	Min	Max
10% grains passed d_{10} (mm)	0.19	0.25	0.70	1.00	0.12	0.13
60% grains passed d_{60} (mm)	1.31	1.87	2.35	2.15	0.29	0.31
Uniformity index U ()	6.9	7.5	3.1	2.4	2.4	2.4
Hydraulic conductivity K (m s^{-1})	2.9×10^{-3b}	5.0×10^{-3b}	5.7×10^{-2a}	1.2×10^{-1a}	1.2×10^{-3b}	2.0×10^{-3a}
Volumetric heat capacity c_{pm} (MJ m^{-3} K^{-1})	2.73	2.73	2.84	2.84	2.93	2.93
Thermal conductivity λ_m (W m^{-1} K^{-1})	2.02	2.24	2.14	2.36	1.87	2.07

[a]Determined by method of *Hazen* [1893].
[b]Determined by method of *Beyer* [1964].

thermal dispersivity compares to solute dispersivity [*Rau et al*., 2012]. *Vandenbohede et al*. [2009] and *Bear* [1988] suspect that thermal is smaller than solute dispersivity, because heat propagates through the solid phase and the pore channels. In contrast, *de Marsily* [1986] found no differences in a combined solute and thermal tracer test. For our application, we suppose limited knowledge of appropriate dispersivity values, and therefore, estimate the longitudinal dispersivity value based on the empirical relationship provided by *Neuman* [1990]:

$$\alpha_l = 0.017 L_s^{1.5} \approx 0.017 (v_{th} t_{TRT})^{1.5} \qquad (12)$$

where the travel distance L_s is assumed to be equal to the product of the effective heat transport velocity, v_{th}, and the duration of the TRT, t_{TRT}. The travel distance can also represent the distance between the source and the observation point. For application purposes, we consider a range for the travel distance, with the borehole radius as the lower bound and the travel distance as upper bound.

[26] While heat transport in the ambient ground is described in detail, heat transport inside the borehole is approximated by one parameter, the thermal borehole resistance, R_b. It relates the temperature difference between the heat carrier fluid and the borehole wall with the applied heat input rate per unit length. There are several approaches to estimate R_b based on the geometry and the material properties of the BHE [e.g., *Sharqawy et al*., 2009a; *Lamarche et al*., 2010]. *Bennet et al*. [1987] introduced the common multipole method. In this study, realistic R_b values are estimated using the multipole method implemented in the simulation software Earth Energy Designer (EED) [*Hellström and Sanner*, 2000]. Ranges are generated based on the known material properties of the BHE (pipe and backfilling material, heat carrier fluid), the operation mode (volume flow rate of the heat carrier fluid and heat injection rate) and the geometry of the BHE (borehole radius, outer/inner pipe radius, number of pipes). The shank spacing, that is, the distance between the centers of the pipes in the borehole, is another unknown. Analogous to the work by *Acuña and Palm* [2009], the full range of feasible shank spacing variants is covered, from one extreme, where all pipes have direct contact in the center of the borehole, to the other, where all pipes are symmetrically distributed at the borehole wall, to obtain the range of feasible R_b values.

2.3. Experimental Setup

[27] Two experiments were conducted to examine the suitability of the TRT for estimating Darcy velocity and

deducing integral hydraulic conductivity. The first one is a well-controlled large-scale tank experiment. Here, all crucial hydraulic and thermal transport parameters are known or can be precisely determined. This experiment serves for validation of the moving line source-based interpretation of monitored thermal response on the laboratory scale. However, laboratory experiments only approximate real in situ conditions. There are often limitations due to boundary or scaling effects, which might influence the results. Thus, the second experiment is a TRT performed at field scale, with moderate knowledge of the thermal and hydraulic parameters of the subsurface. We adopt this to validate our suggested approach at the field scale.

2.3.1. Tank Experiment

[28] A TRT tank experiment with a layered artificial aquifer was conducted at the research facility for subsurface remediation (VEGAS) at the University of Stuttgart (Figure 5). Four grouted boreholes equipped with double U-tubes, which act as BHEs are installed in a water-saturated sand container of 9 m length, 6 m width, and 4.5 m depth. The BHEs, with a radius of 0.1 m, penetrate the upper 4.3 m and, when ignoring the missing 20 cm on the bottom, can be approximated as fully penetrating. Due to the downscaling of this experiment, the length-width ratio of the used BHE (length/width = 4.3 m/0.2 m = 21.5) is rather small. A second critical aspect of the laboratory experiment is the vicinity of the container bottom to the BHE, which might cause unsolicited boundary effects. From these BHEs, one is selected to conduct the TRT. It is located approximately 6 m away from the inflow boundary and approximately at the centerline of the container. The other BHEs are not used but implemented for other experiments [*Wagner et al*., 2012b]. To ensure an optimal thermal connection between BHE and the subsurface, a thermally enhanced grouting material is selected (GWE ThermoSeal®). Comparable to a standard TRT, tap water is taken as heat carrier fluid in the tubes. For this setting, the steady state multipole method delivers R_b ranges between 0.04 and 0.10 m K W^{-1}, considering a shank spacing range from 0 to 0.168 m.

[29] Through controlled inflow and outflow devices, a constant hydraulic gradient can be established in the tank. For the TRT experiment, it is adjusted to 0.003. The artificial aquifer is composed of pure unconsolidated quartz of different well-sorted grain sizes. The five different layers, one of fine sand, two of middle sand, and one of coarse sand, are subhorizontal with an inclination of 3°. The structure is illustrated in Figure 5, and detailed properties of the layers are listed in Table 1. The measured porosity of the
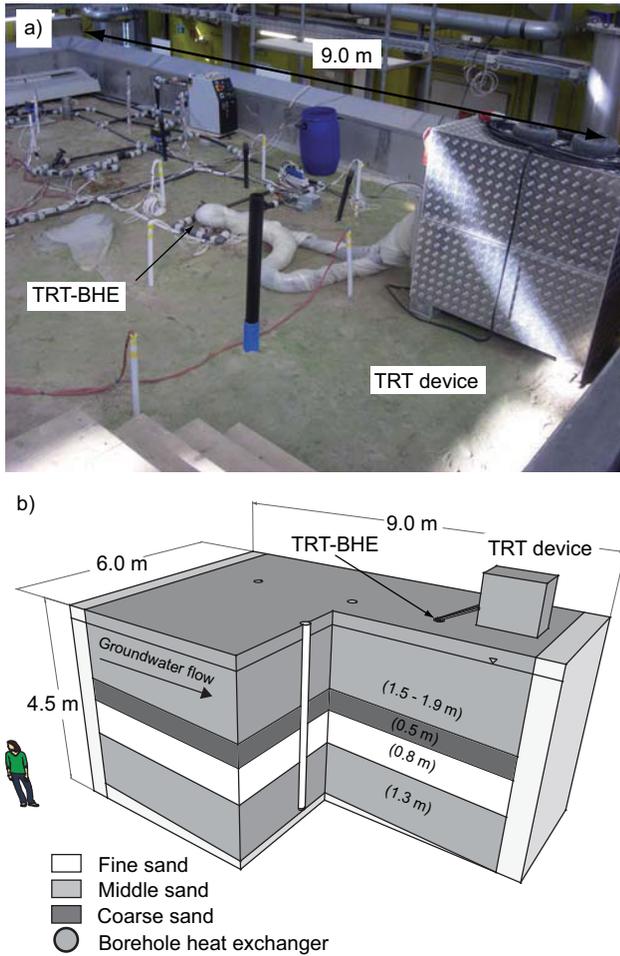
Figure 5. (a) Picture of the tank experiment and (b) schematic bird's eye view of the layered structure and geometries including the thicknesses of the layers.

Figure 6. Grain size distribution from repeated sieve analyses of the three different sandy materials of the tank experiment.

influences, the sensors were positioned directly at the inflow and outflow of the BHE. The TRT was divided in two separate phases. During the initial heating phase of 3 days a constant heat load of 130 W m^{-1} was applied. Then, the behavior during a 5 day recovery phase with no heat load was monitored. The recorded temperature development during the entire TRT is presented in Figure 7.

[32] Evaluation based on equation (6) assumes a homogenous aquifer. To be able to examine the applicability of the presented approach, integral parameters of the artificial aquifer are quantified. Water flow and heat propagation is nearly parallel to the subhorizontal layering, and therefore, an equivalent homogenous media can be calculated by the arithmetic means of the layer properties (Table 2). Based

fine sand layer is 0.40, the middle and coarse sand layers exhibit a porosity of 0.36. Hydraulic conductivity, K, ranges for the three different sand classes are determined by sieve curve analyses (Figure 6) based on the empirical methods by *Hazen* [1893] and *Beyer* [1964]. For each layer, three different samples are analyzed. According to the validity ranges of these methods, the method by *Hazen* [1893] was solely applied for the coarse sand layer, and the method by *Beyer* [1964] was used for the middle sand layers. For the fine sand layer, both methods are valid, and therefore, the widest resulting parameter range considering both methods is selected.

[30] Thermal conductivity of each layer is determined by laboratory measurements using the "TK04 thermal conductivity meter," which is based on the line source method [*Blackwell*, 1954] with a measurement error of ±5%. Due to the fact that each layer is built up of pure quartz sand, the volumetric heat capacity c_{pm} can be reliably calculated by a weighted arithmetic average of volumetric fraction of water and solid [e.g., *Parr et al.*, 1983; *Palmer et al.*, 1992; *Markle et al.*, 2006] (Table 1).

[31] A TRT was employed for a period of 8 days. During the test, sensors recorded the temperature of the heat carrier fluid at 1 minute resolution. To minimize the atmospheric
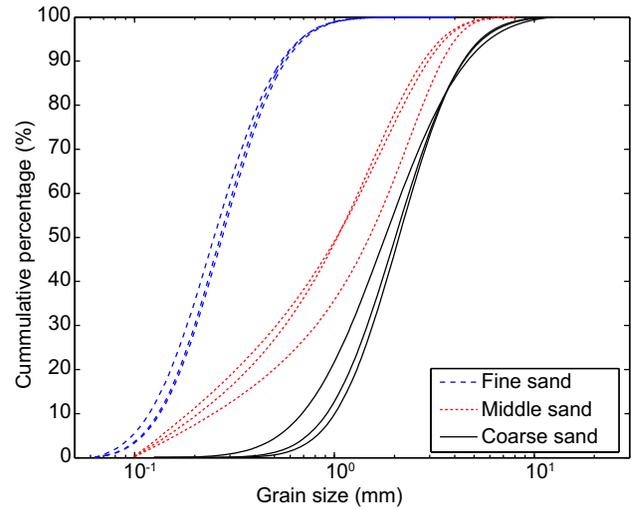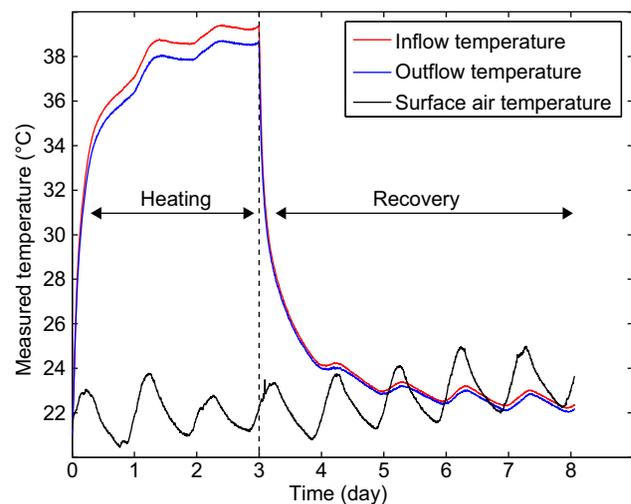

Figure 7. Measured temperature development of the heat carrier fluid temperature at the inflow and outflow of the BHE during the TRT experiment at the tank experiment. Additionally, the air temperature in 0.1 m above the surface is shown.

Table 2. Integral Value Ranges of Hydraulic and Thermal Parameters for the Artificial Aquifer of the Tank Experiment

	Value Range	
	Min	Max
Hydraulic conductivity K (m s^{-1})	8.6×10^{-4}	1.7×10^{-3}
Volumetric heat capacity c_{pm} (J m^{-3} K^{-1})	2.5×10^{6}	3.06×10^{6}
Thermal conductivity λ_m (W m^{-1} K^{-1})	1.64	2.74
Longitudinal dispersivity, α_l (m)	0	0.5
Thermal borehole resistance, R_b (m K W^{-1})	0.04	0.10

on the minimum and maximum observed values, property ranges of the equivalent homogenous media are calculated. For the thermal conductivity, ± 0.55 W m^{-1} K^{-1} ranges are listed in Table 2, which are typical for natural porous aquifers. Although the measurement error of the determined thermal conductivity values is evidently below this range (± 0.11 W m^{-1} K^{-1}), we applied the wider parameter range (± 0.55 W m^{-1} K^{-1}) to inspect the robustness of the parameter estimation procedure. Ranges of the thermal dispersivity values α_l are estimated by equation (12). The minimum travel distance of this experiment is the borehole radius ($r_{bw} = 0.1$ m), and the maximum travel distance is limited by the size of the tank, which is 9 m. We obtain a longitudinal dispersivity ranging between 0 and 0.5 m with the resulting transversal dispersivity using the commonly applied 1/10 of α_l.

2.3.2. Field Experiment

[33] In addition to the tank experiment, we examine also a field site in the upper Rhine valley at the town of Schwanau in southwest Germany. One vertical borehole of 0.14 m diameter, with double U-tube pipes, was installed to a depth of 100 m (Figure 8). The length-width ratio of the field-scale BHE (length/width = 100 m/0.2 m = 500) is clearly higher than the one of the tank experiment. It is grouted with thermally enhanced grouting material (ZEO Therm 2.0 from the company Hans G. Hauri KG). Borehole resistance ranges are determined by the multipole-based method, analog to the procedure for the tank experiment, considering a shank spacing range from 0 to 0.108 m. The derived R_b ranges vary between 0.04 and 0.09 m K W^{-1}. The BHE fully penetrates an aquifer with a thickness of 68 m and partially intersects an underlying low-permeability formation, which is made up of sandstone and claystone units (Figure 8). The aquifer is composed of flood plain and low terrace gravel. The low-permeability formation consists of one 15 m thick claystone layer embedded in two sandstone layers with a total thickness of 17 m. According to *Junker and Essler* [1980], the hydraulic conductivity, K, of the aquifer, which is allocated to the so-called upper and middle gravel layers of the Rhine valley, varies between 2.3×10^{-3} and 1.2×10^{-2} m s^{-1}. These values were obtained by several sieve curve analyses and hydraulic pumping tests. No specific hydraulic data are available for the low-permeability formation. With a typical value range of 10^{-6} to 10^{-9} m s^{-1} for sandstones and $<10^{-9}$ m s^{-1} for
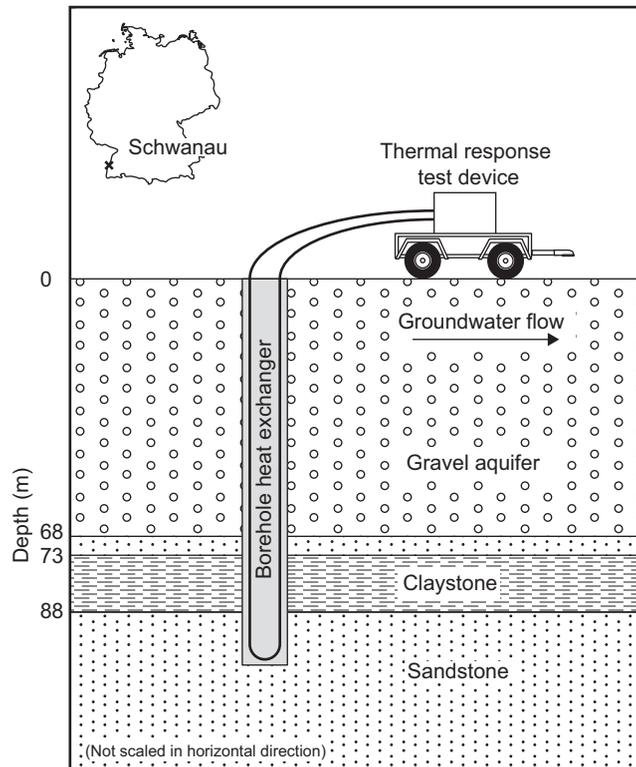

Figure 8. Schematic cross section of the studied field experiment in Schwanau (Germany) showing the layered geological units. The individual depths of the layer boundaries are determined based on borehole cuttings. The depth to water table is only 2 m and is therefore, not explicitly shown.
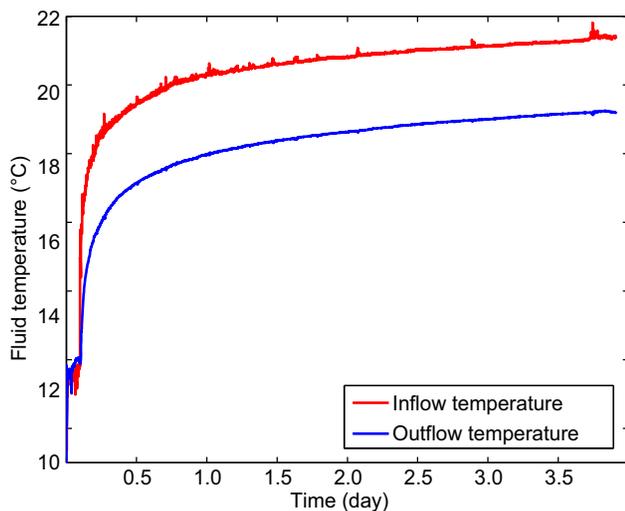
Table 3. Properties of the Different Geological Layers for the Field Site

| | Aquifer | | Low-Permeability Formation | | | |
| | Porous Media | | Sandstone | | Claystone | |
	Min	Max	Min	Max	Min	Max
Hydraulic conductivity K (m s^{-1})	2.3×10^{-3}	12×10^{-3}	$<1 \times 10^{-9}$	1×10^{-6}	$<1 \times 10^{-9}$	1×10^{-6}
Volumetric heat capacity c_{pm} (MJ m^{-3} K^{-1})	2.51	3.07	2.05	2.05	2.30	2.30
Thermal conductivity λ_m (W m^{-1} K^{-1})	1.64	2.74	3.77	3.77	1.05	1.05

clays [*Domenico and Schwartz*, 1998], a parameter range of 10^{-6} to $<10^{-9}$ m s^{-1} is considered here for the hard rocks below the aquifer.

[34] At the field site, thermal parameters are not specifically investigated by additional laboratory experiments. Thus, empirical ranges of the volumetric heat capacity and the thermal conductivity, based on reported data, have to be defined here (Table 3). The volumetric heat capacity of a natural porous aquifer is typically about 2.79 MJ m^{-3} K^{-1}, with a variability of ± 0.28 MJ m^{-3} K^{-1}. A thermal conductivity range from 1.64 to 2.74 W m^{-1} K^{-1}, with a mean value of 2.20 W m^{-1} K^{-1} is assumed for the aquifer material. Volumetric heat capacities of the low-permeability formation are estimated based on the study by *Clauser* [2011], and the thermal conductivities of the sandstone and the claystone are extracted from *Domenico and Schwartz* [1998].

[35] The TRT started on the 28th of January 2010 and lasted for 4 days. A mobile device was used, which applied power-controlled continuous-flow heaters to reach a constant heat injection rate of 49.3 W m^{-1} during the experiment. The heat carrier fluid was tap water. Flow rates, inlet and outlet temperatures of the fluid in each U-pipe loop were continuously monitored. The testing time can be separated in an initial burn-in phase, where only fluid circulates without any heat injection (0.1 day) and a second constant heating phase. The recorded temperature curves of the fluid at the inlet and outlet of the BHE are shown in Figure 9. The irregular temperature fluctuations at the inlet fluid temperature are caused by slight instabilities of the chosen fluid flow rate and/or irregularities in the power net supply. In contrast to observations at the tank experiment, atmospheric diurnal temperature fluctuations have no noticeable influence. This is attributed to different measurement devices, as well as to the larger BHE depth and size of the field-scale TRT.

[36] We follow the same procedure as for the tank experiment, and average the hydraulic and thermal values assuming an equivalent homogenous medium. Based on the thicknesses of the porous aquifer, sandstone and the clay layer, the weighted arithmetic mean of the hydraulic and thermal parameters is calculated. The derived ranges serve as input for equation (6), except of the hydraulic conductivity, which is utilized for validation (Table 4). Ranges of thermal dispersivity are determined based on equation (12). The borehole radius of the BHE represents the minimum travel distance for this experiment, which is $r_{bw} = 0.065$ m. The maximum travel distance ($L_s = 5.9$ m) is calculated based on the expected effective heat transport velocity ($v_{th} = 1.7 \times 10^{-5}$ m s^{-1}) and the duration of the TRT ($t = 4$ days). Longitudinal dispersivity values are determined by equation (12) and the obtained range varies between 0 and 0.24 m. The transversal dispersivity is set to one-tenth of the longitudinal dispersivity.

3. Results and Discussion

3.1. Interpretation of the Tank Experiment

[37] The undulating inlet and outlet heat carrier fluid temperatures of the tank experiment (Figure 7) are averaged for TRT interpretation (Figure 10). By superposition of phases with specific heat loads q_t, equation (6) facilitates simulations of the two time periods of heating ($q_n = 130$ W m^{-1}, $t = 0$–3 days) and recovery ($q_n = 0$, $t = 3$–8 days). The parameter estimation step follows the scheme as illustrated in Figure 3, and this means that exclusively v_{eff} is iteratively optimized. The evaluation interval considered for the parameter estimation is set to 0.8–7.0 days. All other thermal transport parameters λ_m, c_{pm}, α_l, and the thermal borehole resistance, R_b, are considered uncertain

Figure 9. Measured inflow and outflow temperatures of the heat carrier fluid during TRT at Schwanau field site.

Table 4. Integral Values of Thermal and Hydraulic Parameters at the Field Site

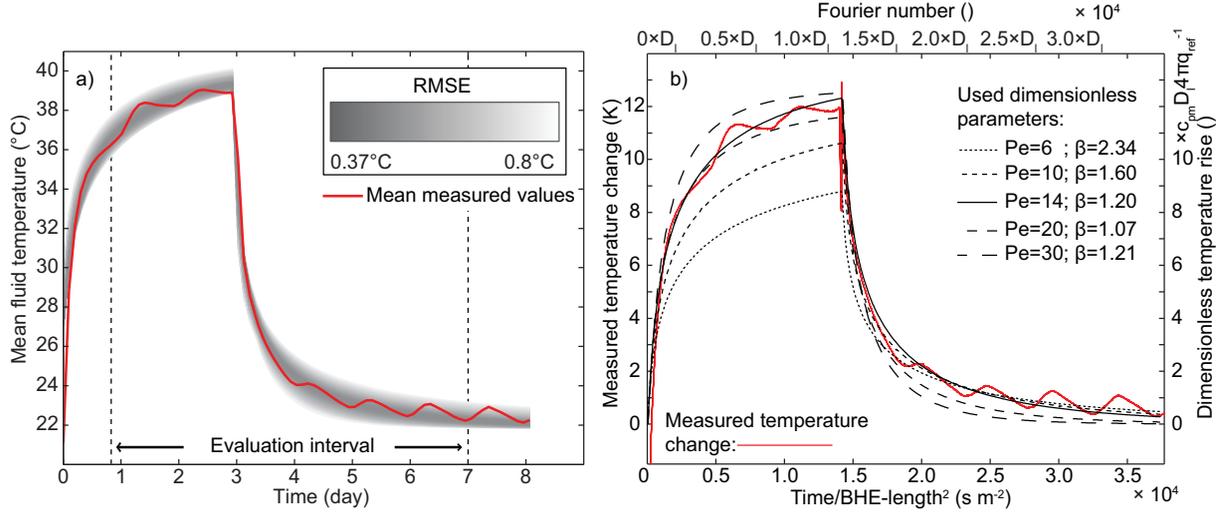| | Value Range | |
	Min	Max
Hydraulic conductivity K (m s^{-1})	1.6×10^{-3}	8.3×10^{-3}
Volumetric heat capacity c_{pm} (J m^{-3} K^{-1})	2.40×10^{6}	2.79×10^{6}
Thermal conductivity λ_m (W m^{-1} K^{-1})	1.90	2.66
Longitudinal dispersivity, α_l (m)	0	0.24
Thermal borehole resistance, R_b (m K W^{-1})	0.04	0.09

Figure 10. Fitting results of the tank experiment. (a) Comparison of mean measured fluid temperature and results of the parameter estimation approach based on equation (6). (b) Comparison of the measured temperature change and a set of calculated universal temperature response curves based on equation (7). For straightforward comparison between measured and simulated data, the nondimensionalization is executed by multiplying $t\,H^{-1}$ with D_l to result in the Fourier number and by multiplying ΔT with $c_{pm}\,D_l\,4\,\pi\,q_{ref}^{-1}$ to determine the dimensionless temperature rise.

within the given ranges listed in Table 2. Note that the uncertainty is significant, for instance, within ±40% for R_b. These ranges are discretized in 10 steps for each parameter, and for each of the possible parameters permutations (total number of $(10)^4 = 10,000$), v_{eff} is calibrated. This procedure offers detailed insights into feasible parameter value pairs. Feasibility is defined by a fitting error threshold, which is set here after preliminary visible inspection of fitted curves with RMSE = 0.8°C. This tolerance takes into account that often no unique solution exists or is searched for, and it respects potential measurement errors and noise. In the tank experiment substantial noise is apparently introduced by the influence of the diurnal atmospheric temperature variability, and the low BHE length-width ratio might also cause some imprecisions. Measurement error by the PT100 sensors is only ±0.1°C.

[38] Best fit result is an apparent global optimum, RMSE = 0.37°C, with $\lambda_m = 2.61$ W m^{-1} K^{-1}, $c_{pm} = 2.56 \times 10^6$ J m^{-3} K^{-1}, $\alpha_l = 0.06$ m and with a thermal borehole resistance, $R_b = 0.040$ m K W^{-1}. However, Figure 10a reveals a large number of about 2900 (29% of all trials) of feasible suboptimal solutions. The simulated temperature trends span the grey shadow surrounding the measured temperatures. As illustrated in Figure 10a, the threshold of 0.8°C is chosen to encompass the entire undulating curve from the measurement.

[39] Based on the solution-specific thermal conductivity and the determined v_{eff}, the corresponding correction factors (Figure 2) are selected to derive the (average) Darcy velocity, v. Since the hydraulic gradient of the experiment is known ($i = 0.003$), based on Darcy's law, an integral hydraulic conductivity, K, of the artificial aquifer can be obtained. The values of all possible solutions with their respective fitting errors are shown in Figure 11. The global optimum of $K = 0.9 \times 10^{-3}$ m s^{-1} is close to the mean of the range determined from the sieve analysis with $K = 1.3$

$\times 10^{-3}$ m s^{-1} (Table 2). The point cloud of solutions spans a wide range of resulting hydraulic conductivity values, but this shows an overall best fitting in the range of the sieve curve results and this is the most striking feature. Thus, the TRT-based estimation coincides well with the hydraulic characterization based on this hydrogeological standard technique, despite the high uncertainty of the thermal parameters. This indicates that the developed evaluation approach is very robust.

[40] For a dimensionless analysis of the results, equation (7) is applied. Five pairs of the dimensionless variables Pe and β are chosen, consistent with the parameter ranges
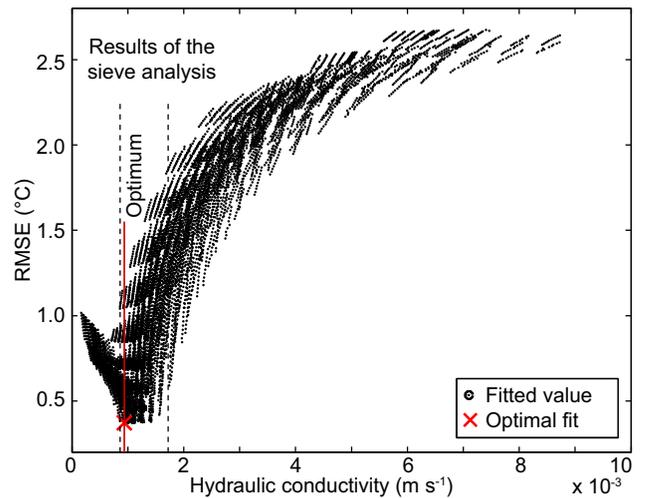

Figure 11. Hydraulic conductivity values obtained from the determined corrected effective Darcy velocity, and the corresponding RMSE value of the performed parameter estimation approach.
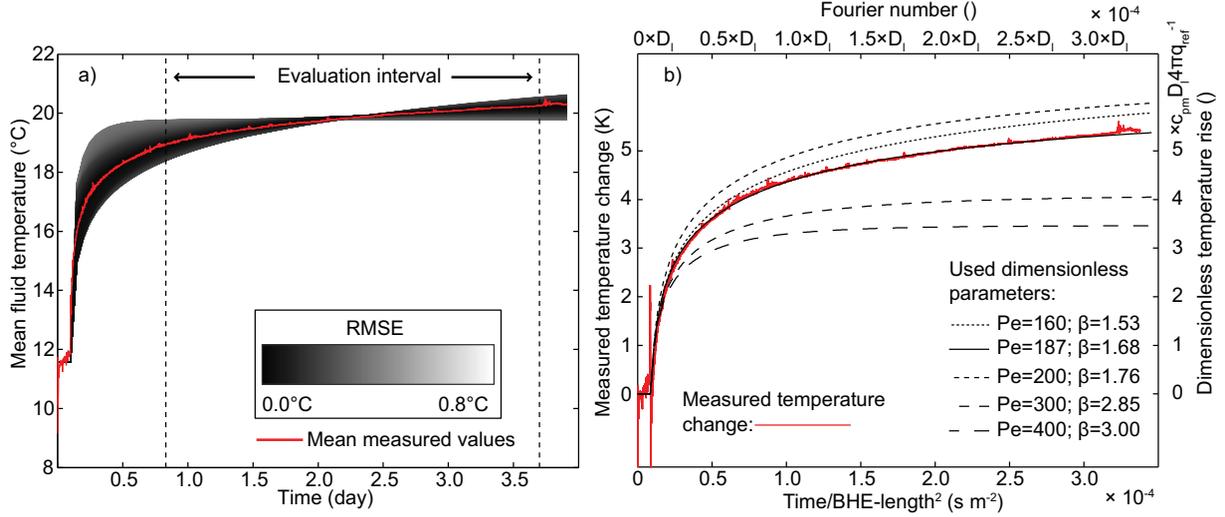
Figure 12. Fitting results of the field experiment. (a) Comparison of the measured mean fluid temperature and the results of the parameter estimation approach based on equation (6). (b) Comparison of the measured temperature change and a set of calculated universal temperature response curves based on equation (7). For straightforward comparison between measured and simulated data, the nondimensionalization is executed by multiplying $t H^{-1}$ with D_l to result in the Fourier number and by multiplying ΔT with $c_{pm} D_l 4 \pi q_{ref}^{-1}$ to determine the dimensionless temperature rise.

determined for the tank experiment (Table 2). *Pe* numbers range from 6 to 30, and β values range from 1.07 to 2.34, which cover the value domain surrounding the best-fitted *Pe* and β combinations. Based on these pairs, a set of five universal thermal response curves are determined and compared to the measured temperature changes of the TRT experiment. This comparison is presented in Figure 10b for a fixed $R_b = 0.04$ m K W^{-1}, which represents the R_b value used to obtain the best fit result of the dimensional formulation of the moving line source.

[41] The most suitable pair (*Pe* $=14$; $\beta = 1.20$) is also in accordance to the best fit. The dimensionless analysis also reveals the correlation between the four parameters (λ_m, c_{pm}, α_l, and v, respectively, K), suitable to model the observed thermal response of the subsurface. Furthermore, if thermal dispersion is neglected or assumed to be isotropic, i.e., β becomes 1, and the heat transport in the subsurface depends only on *Pe*. For this simplification, a unique *Pe* number can be determined and used to derive possible K values based on the predefined thermal parameter ranges, instead of applying a multiparameter estimation procedure.

3.2. Interpretation of the Field Experiment

[42] The temperature time series measured during the field TRT are employed to validate the introduced parameter estimation approach at the field scale (Figure 9). First, equivalent to the procedure for the tank experiment, the mean of inlet and outlet heat carrier fluid temperature is computed and plotted in Figure 12. Then, burn-in phase ($q_n = 0$ W m^{-1}, $t = 0$–0.1 days) and heating period ($q_n = 49.3$ W m^{-1}, $t = 0.1$–3.9 days) are superimposed based on equation (6). The evaluation interval is set from 0.8 to 3.7 days after initiation temperature recording. Again, v_{eff} is iteratively optimized, while the 10 discretization steps within the ranges listed in Table 4 are applied for all other relevant parameters (λ_m, c_{pm}, α_l, and R_b). The

fitting error threshold is not changed from the tank experiment and kept at 0.8°C.

[43] In comparison to the tank experiment, the influence of diurnal temperature variations is not significant for this experiment; therefore, better agreement between mean measured and simulated temperatures is achieved. In fact, all parameter variations result in a misfit below the RMSE threshold. This indicates that within the range of noise and measurement error, a large number of acceptable solutions exist. The best result is obtained for a parameter combination of $\lambda_m = 2.66$ W m^{-1} K^{-1}, $c_{pm} = 2.53 \times 10^6$ J m^{-3} K^{-1}, $\alpha_l = 0.24$ m, and thermal borehole resistance, $R_b = 0.068$ m K W^{-1}, with an RMSE value of 0.021°C.

[44] To obtain the integral hydraulic conductivity of the field site, in a first step, the corresponding values of the correction factor are determined. With this factor, the fitted v_{eff} values are transferred to the actual integral Darcy velocity v (equation (8)). Applying Darcy's law and taking the known hydraulic gradient of 0.001, the integral values of K are determined for all fitting trials. In Figure 13, the derived K values are plotted versus the fitting errors. The best result, with a misfit of 0.021°C, yields $K = 3.1 \times 10^{-3}$ m s^{-1}. This value is within the K range determined by sieve analysis and pumping tests for this site, which reaches from 1.6×10^{-3} to 8.3×10^{-3} m s^{-1} (Table 4). Furthermore, by comparing all obtained results, a distinct optimal interval can be determined, which is also within the range of K values determined from the study of *Junker and Essler* [1980]. This optimal interval, where RMSE < 0.05°C, reaches from 2.5×10^{-3} to 5.5×10^{-3} m s^{-1}. This demonstrates for the field scale, that the TRT data can also be applied to determine hydraulic conductivity values comparable to the ones obtained from standard hydraulic investigation methods such as hydraulic pumping tests or sieve curve analysis. A premise is that the weighted arithmetic mean is applied to consider a layered structure of the
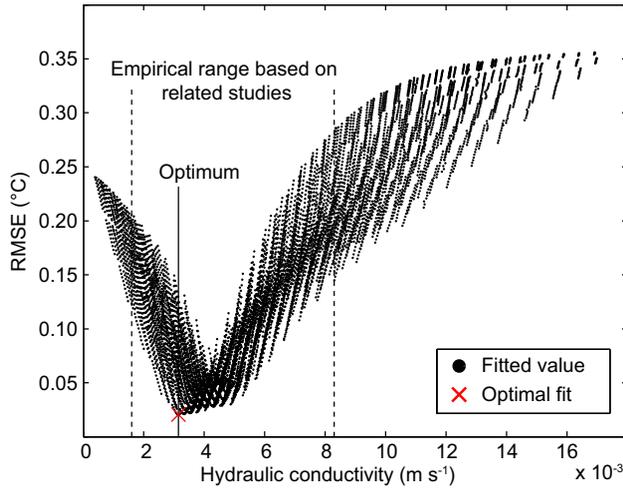
Figure 13. Hydraulic conductivity, K, values obtained from the determined corrected effective Darcy velocity and the corresponding RMSE value of the performed parameter estimation approach. Empirical range is extracted from Table 4.

subsurface including penetrated aquifer and low-permeability formation. It is noteworthy that the Schwanau experiment was merely conducted to support the design of a larger ground source heat pump (GSHP) system; hence, it clearly demonstrates that the developed procedure can be confidently applied to determine hydraulic parameters.

[45] Following the same procedure as for the tank experiment, five pairs of Pe and β are selected for dimensionless analysis of the results. Based on the best fit result of the dimensional analysis and the specified parameter ranges (Table 4), Pe and β pairs are defined to cover the corresponding dimensionless parameter array. For the field site, these cover the intervals $160 \leq Pe \leq 400$ and $1.53 \leq \beta \leq 3.00$. The R_b is set to 0.068 m K W^{-1}, which represents the value associated with the previously determined best-fitted K value.

[46] As expected, the dimensionless analysis shown in Figure 12b exhibit the best agreement of the measured and calculated temperature for the parameter pair ($Pe = 187$; $\beta = 1.68$) obtained from the best fit of the dimensional analysis. The dimensionless formulation results in a reduced number of heat transport relevant parameters of the subsurface, two (Pe and β) instead of four (λ_m, c_{pm}, α_l, and v, respectively, K). Thus, the heat transport behavior can be expressed in a more condensed formulation. Nevertheless, there are still two relevant subsurface parameters, which allow for the determination of one unique Pe number compiling the correlation of the four-dimensional heat transport parameters λ_m, c_{pm}, α_l, and v, respectively, K. Hence, the dimensionless formulation provides a suitable and condensed description of the parameter correlation, but the major objective, to determine the hydraulic conductivity, cannot be further improved by applying a dimensionless formulation.

4. Summary and Conclusions

[47] Hydraulic characterization of the subsurface is a major task of hydrogeological field methods. This study proposes an advection sensitive TRT evaluation as a potential method to estimate Darcy velocity and integral aquifer hydraulic conductivity. For demonstrating the applicability, the correction term-based TRT evaluation by *Wagner et al.* [2013] is integrated in a two-step fitting approach. Two measured TRT temperature time series, from a large-scale tank experiment and one from a standard field TRT are used to validate the new approach. Results for both experiments reveal that temperature time series of a TRT can be assuredly used to determine hydraulic parameters. This is feasible in spite of (i) the conceptual shortcomings of the simplified line source model, (ii) the high uncertainty in crucial thermal parameter values, and (iii) the noise typically overprinting measurement data.

[48] In principle, the used infinite moving line source model is only applicable to homogeneous conditions, and it does not properly describe the flow and transport processes close to and inside the BHE. As demonstrated, even if heterogeneity cannot be resolved, an integral value of depth averaged Darcy velocity can be obtained. This is a precious insight, comparable to the one obtained by pumping tests. In comparison, however, TRTs are closed applications without mass exchange, with little minor lateral and high axial range. Depth averaging integrates properties of unsaturated zone, aquifer and low-permeability formation. An extension to facilitate also depth-dependent evaluation would be a DTS system with an integrated heating wire in the BHE-like enhanced TRT [e.g. *Fujii et al.*, 2009; *Acuña*, 2013]. By the same heat injection in different layers or compartments, the thermal response would allow distinguishing high from low-velocity zones.

[49] Simulation of heat transport at the BHE is improved by using superimposed line source equations. The most critical aspect is the lateral heterogeneity due to the discrepancy between grout and ground conductivity. By introducing a versatile correction factor that increases with estimated effective thermal conductivity and decreases with estimated effective Darcy velocity, this hurdle is overcome and robust parameter estimation is developed. Improvement potential lies in the applied line source model. Especially for shorter boreholes, a favorable choice is the finite moving line source model developed by *Molina-Giraldo et al.* [2011b]. This variant also considers axial effects, and can be applied at similar computational effort. However, for conditions with substantial axial effects, the correction factor has not been employed, yet, and may need to be adjusted.

[50] Despite the promising results, constructing a BHE and performing a TRT to exclusively characterize hydrogeology is not often favorable, because of the large involved investment costs for constructing a BHE and performance of the TRT. Instead, the potential of the new method is to complement standard interpretation of TRT. This does not only refer to future TRT applications, but we see a high potential in reinterpreting existing temperature time series of the numerous existing TRT applications worldwide, which for example, were conducted associated with the strong geothermal development in Europe during the last decade.

References

Acuña, J. (2013), *Distributed Thermal Response Tests—New Insights on U-Pipe and Coaxial Heat Exchangers in Groundwater-Filled Boreholes*, KTH Sch. of Ind. Eng. Manage., Stockholm.

Acuña, J., and B. Palm (2009), Local conduction heat transfer in U-pipe borehole heat exchangers, paper presented at COMSOL Conference, Milan, Italy.

Anderson, M. P. (2005), Heat as a ground water tracer, *Ground Water*, *43*(6), 951–968, doi:10.1111/j.1745–6584.2005.00052.x.

Angermann, L., S. Krause, and J. Lewandowski (2012), Application of heat pulse injections for investigating shallow hyporheic flow in a lowland river, *Water Resour. Res.*, *48*, W00P02, doi:10.1029/2012WR012564.

Bayer, P., and M. Finkel (2007), Optimization of concentration control by evolution strategies: Formulation, application, and assessment of remedial solutions, *Water Resour. Res.*, *43*, W02410, doi:10.1029/2005WR004753.

Bayer, P., D. Saner, S. Bolay, L. Rybach, and P. Blum (2012), Greenhouse gas emission savings of ground source heat pump systems in Europe: A review, *Renewable Sustainable Energy Rev.*, *16*(2), 1256–1267, doi:10.1016/j.rser.2011.09.027.

Bear, J. (1988), *Dynamics of Fluids in Porous Media*, Dover, Mineola, New York.

Bear, J., and A. Cheng (2010), *Modeling Groundwater Flow and Contaminant Transport*, Springer and Bus. Media B.V., Dordrecht.

Bennet, J., J. Claesson, and G. Hellström (1987), Multipole method to compute the conductive heat flows to and between pipes in a composite cylinder, *Notes on Heat Transfer 3–1987*, Dep. of Building Technol. and Dep. of Math. Phys., Lund Inst. of Technol., Lund, Sweden.

Beyer, W. (1964), Zur Bestimmung der Wasserdurchlässigkeit von Kiesen und Sanden aus der Kornverteilung, *Wasserwirt. Wassertech.*, *14*, 165–169.

Blackwell, J. H. (1954), A transient-flow method for determination of thermal constants of insulating materials in bulk part I—Theory, *J. Appl. Phys.*, *25*(2), 137–144.

Blum, P., G. Campillo, and T. Kölbel (2011), Techno-economic and spatial analysis of vertical ground source heat pump systems in Germany, *Energy*, *36*(5), 3002–3011, doi:10.1016/j.energy.2011.02.044.

Bravo, H. R., F. Jiang, and R. J. Hunt (2002), Using groundwater temperature data to constrain parameter estimation in a groundwater flow model of a wetland system, *Water Resour. Res.*, *38*(8), 1153, doi:10.1029/2000WR000172.

Byrne, G. F., J. E. Drummond, and C. W. Rose (1967), A sensor for water flux in soil. "Point source" instrument, *Water Resour. Res.*, *3*(4), 1073–1078, doi:10.1029/WR003i004p01073.

Cardenas, M. B. (2010), Thermal skin effect of pipes in streambeds and its implications on groundwater flux estimation using diurnal temperature signals, *Water Resour. Res.*, *46*, W03536, doi:10.1029/2009WR008528.

Carslaw, H. S., and J. C. Jaeger (1959), *Conduction of Heat in Solids*, 2nd ed., 510 pp., Clarendon, Oxford.

Chiasson, A., and A. O'Connell (2011), New analytical solution for sizing vertical borehole ground heat exchangers in environments with significant groundwater flow: Parameter estimation from thermal response test data, *HVAC&R Res.*, *17*(6), 1000–1011.

Clauser, C. (2011), Thermal storage and transport properties of rocks, I: Heat capacity and latent heat, in *Encyclopedia of Solid Earth Geophysics*, edited by H. Gupta, pp. 1423–1431, Springer, Netherlands.

de Marsily, G. (1986), *Quantitative Hydrogeology: Groundwater Hydrology for Engineers*, Academic Press, Orlando, Fla.

de Vries, D. (1963), Thermal properties of soils, in *Physics of the Plant Environment*, edited by W. R. Van Wijk, North-Holland, Amsterdam.

Diersch, H. J. G. (2009), *FEFLOW User's Manual*, WASY GmbH, Berlin.

Domenico, P. A., and F. W. Schwartz (1998), *Physical and Chemical Hydrogeology*, 2nd ed., John Wiley, Chichester, United Kingdom.

Fetter, C. W. (2001), *Applied Hydrogeology*, 4th ed., Prentice Hall, Upper Saddle River, N. J.

Fujii, H., H. Okubo, K. Nishi, R. Itoi, K. Ohyama, and K. Shibata (2009), An improved thermal response test for U-tube ground heat exchanger based on optical fiber thermometers, *Geothermics*, *38*(4), 399–406, doi:10.1016/j.geothermics.2009.06.002.

Gao, J., T. Ren, and Y. Gong (2006), Correcting wall flow effect improves the heat-pulse technique for determining water flux in saturated soils, *Soil Sci. Soc. Am. J.*, *70*(3), 711–717, doi:10.2136/sssaj2005.0174.

Gehlin, S. (2002), Thermal response test method development and evaluation, PhD thesis, Luleå Univ. of Technol., Luleå, Sweden.

Gelhar, L. W., C. Welty, and K. R. Rehfeldt (1992), A critical review of data on field-scale dispersion in aquifers, *Water Resour. Res.*, *28*(7), 1955–1974, doi:10.1029/92WR00607.

Greswell, R. B., M. S. Riley, P. F. Alves, and J. H. Tellam (2009), A heat perturbation flow meter for application in soft sediments, *J. Hydrol.*, *370*(1–4), 73–82, doi:10.1016/j.jhydrol.2009.02.054.

Hazen, A. (1893), Some physical properties of sand and gravels with special reference to their use in filtration, report, 539–556 pp., Mass. State Board of Health, Boston.

Hecht-Méndez, J., N. Molina-Giraldo, P. Blum, and P. Bayer (2010), Evaluating MT3DMS for heat transport simulation of closed geothermal systems, *Ground Water*, *48*(5), 741–756, doi:10.1111/j.1745–6584.2010.00678.x.

Hellström, G., and B. Sanner (2000), *Earth Energy Designer-EED*, Version 2.0. Blocon Sweden, Lund, Sweden.

Hopmans, J. W., J. Šimunek, and K. L. Bristow (2002), Indirect estimation of soil thermal properties and water flux using heat pulse probe measurements: Geometry and dispersion effects, *Water Resour. Res.*, *38*(1), 1006, doi:10.1029/2000WR000071.

Hurtig, E., S. Großwig, M. Jobmann, K. Kühn, and P. Marschall (1994), Fibre-optic temperature measurements in shallow boreholes: Experimental application for fluid logging, *Geothermics*, *23*(4), 355–364, doi:10.1016/0375–6505(94)90030-2.

Junker, B., and H. Essler (1980), Hydrogeologische Karte von Baden-Württemberg, map, scale 1:50 000 (dHGK), Hydrogeologische Karte Lahr. Landesamt für Geologie, Rohstoffe und Bergbau Baden Württemberg, Freiburg, Germany.

Klepikova, M. V., T. Le Borgne, O. Bour, P. Davy (2011), A methodology for using borehole temperature-depth profiles under ambient, single and cross-borehole pumping conditions to estimate fracture hydraulic properties, *J Hydrol*, *407*(1–4), 145–152, doi: 10.1016/j.jhydrol.2011.07.018.

Lagarias, J. C., J. A. Reeds, M. H. Wright, and P. E. Wright (1998), Convergence properties of the Nelder-Mead simplex method in low dimensions, *Siam J. Optim.*, *9*(1), 112–147.

Lamarche, L., S. Kajl, and B. Beauchamp (2010), A review of methods to evaluate borehole thermal resistances in geothermal heat-pump systems, *Geothermics*, *39*(2), 187–200, doi:10.1016/j.geothermics.2010.03.003.

Lautz, L. K. (2010), Impacts of nonideal field conditions on vertical water velocity estimates from streambed temperature time series, *Water Resour. Res.*, *46*, W01509, doi:10.1029/2009WR007917.

Ma, R., C. Zheng, J. M. Zachara, and M. Tonkin (2012), Utility of bromide and heat tracers for aquifer characterization affected by highly transient flow conditions, *Water Resour. Res.*, *48*, W08523, doi:10.1029/2011WR011281.

Macfarlane, A., A. Förster, D. Merriam, J. Schrötter, and J. Healey (2002), Monitoring artificially stimulated fluid movement in the Cretaceous Dakota aquifer, Western Kansas, *Hydrogeol. J.*, *10*(6), 662–673, doi:10.1007/s10040-002-0223-7.

Markle, J. M., R. A. Schincariol, J. H. Sass, and J. W. Molson (2006), Characterizing the two-dimensional thermal conductivity distribution in a sand and gravel aquifer, *Soil Sci. Soc. Am. J.*, *70*(4), 1281–1294, doi:10.2136/sssaj2005.0293.

Menberg, K., H. Steger, R. Zorn, M. Reuß, M. Pröll, P. Bayer, and P. Blum (2013), Bestimmung der Wärmeleitfähigkeit im Untergrund durch Labor- und Feldversuche und anhand theoretischer Modelle, *Grundwasser*, *18*, 103–116, doi:10.1007/s00767-012-0217-x.

Mogensen, P. (1983), Fluid to duct wall heat transfer in duct system heat storage, paper presented at the International Conference on Surface Heat Storage in Theory and Practice, Stockholm, Sweden.

Molina-Giraldo, N., P. Bayer, and P. Blum (2011a), Evaluating the influence of thermal dispersion on temperature plumes from geothermal systems using analytical solutions, *Int. J. Therm. Sci.*, *50*(7), 1223–1231, doi:10.1016/j.ijthermalsci.2011.02.004.

Molina-Giraldo, N., P. Blum, K. Zhu, P. Bayer, and Z. Fang (2011b), A moving finite line source model to simulate borehole heat exchangers with groundwater advection, *Int. J. Therm. Sci.*, *50*(12), 2506–2513, doi:10.1016/j.ijthermalsci.2011.06.012.

Nelder, J. A., and R. Mead (1965), A simplex method for function minimization, *Comput. J.*, *7*(4), 308–313, doi:10.1093/comjnl/7.4.308.

Neuman, S. P. (1990), Universal scaling of hydraulic conductivities and dispersivities in geologic media, *Water Resour. Res.*, *26*(8), 1749–1758, doi:10.1029/WR026i008p01749.

Ochsner, T. E., R. Horton, G. J. Kluitenberg, and Q. Wang (2005), Evaluation of the heat pulse ratio method for measuring soil water flux, *Soil Sci. Soc. Am. J.*, *69*(3), 757–765, doi:10.2136/sssaj2004.0278.

Palmer, C. D., D. W. Blowes, E. O. Frind, and J. W. Molson (1992), Thermal energy storage in an unconfined aquifer: 1. Field injection experiment, *Water Resour. Res.*, *28*(10), 2845–2856, doi:10.1029/92WR01471.

Parr, A. D., F. J. Molz, and J. G. Melville (1983), Field determination of aquifer thermal energy storage parameters, *Ground Water*, *21*(1), 22–35, doi:10.1111/j.1745–6584.1983.tb00701.x.

Rau, G. C., M. S. Andersen, and R. I. Acworth (2012), Experimental investigation of the thermal dispersivity term and its significance in the heat transport equation for flow in sediments, *Water Resour. Res.*, *48*, W03511, doi:10.1029/2011WR011038.

Raymond, J., R. Therrien, L. Gosselin, and R. Lefebvre (2011), Numerical analysis of thermal response tests with a groundwater flow and heat transfer model, *Renewable Energy*, *36*(1), 315–324, doi:10.1016/j.renene.2010.06.044.

Saar, M. (2011), Review: Geothermal heat as a tracer of large-scale groundwater flow and as a means to determine permeability fields, *Hydrogeol. J.*, *19*(1), 31–52, doi:10.1007/s10040-010-0657-2.

Sharqawy, M. H., E. M. Mokheimer, and H. M. Badr (2009a), Effective pipe-to-borehole thermal resistance for vertical ground heat exchangers, *Geothermics*, *38*(2), 271–277, doi:10.1016/j.geothermics.2009.02.001.

Sharqawy, M. H., S. A. Said, E. M. Mokheimer, M. A. Habib, H. M. Badr, and N. A. Al-Shayea (2009b), First in situ determination of the ground thermal conductivity for boreholeheat exchanger applications in Saudi Arabia, *Renewable Energy*, *34*(10), 2218–2223, doi:10.1016/j.renene.2009.03.003.

Sharqawy, M. H., H. M. Badr, and E. M. Mokheimer (2013), Investigation of buoyancy effects on heat transfer between a vertical borehole heat exchanger and the ground, *Geothermics*, *48*, 52–59, doi:10.1016/j.geothermics.2013.04.003.

Signorelli, S., S. Bassetti, D. Pahud, and T. Kohl (2007), Numerical evaluation of thermal response tests, *Geothermics*, *36*(2), 141–166, doi:10.1016/j.geothermics.2006.10.006.

Stallman, R. W. (1963), Computation of groundwater velocity from temperature data, *U.S. Geol. Surv. Water Supply Pap.*, *1544*, 36–46.

Sudicky, E. A. (1986), A natural gradient experiment on solute transport in a sand aquifer: Spatial variability of hydraulic conductivity and its role in the dispersion process, *Water Resour. Res.*, *22*(13), 2069–2082, doi:10.1029/WR022i013p02069.

Sutton, M. G., D. W. Nutter, and R. J. Couvillion (2002), A ground resistance for vertical bore heat exchangers with groundwater flow, *ASME J. Energy Resour. Technol.*, *125*, 183–189.

Vandenbohede, A., A. Louwyck, and L. Lebbe (2009), Conservative solute versus heat transport in porous media during push-pull tests, *Transp. Porous Media*, *76*(2), 265–287, doi:10.1007/s11242-008-9246-4.

Wagner, V., P. Bayer, M. Kübert, and P. Blum (2012a), Numerical sensitivity study of thermal response tests, *Renewable Energy*, *41*, 245–253, doi:10.1016/j.renene.2011.11.001.

Wagner, V., P. Bayer, G. Bisch, J. Braun, N. Klaas, and P. Blum (2012b), Calibrating a high-resolution numerical model of a borehole heat exchanger using FEFLOW, paper presented at 3rd International FEFLOW User Conference, Berlin, Germany.

Wagner, V., P. Blum, M. Kübert, and P. Bayer (2013), Analytical approach to groundwater-influenced thermal response tests of grouted borehole heat exchangers, *Geothermics*, *46*, 22–31, doi:10.1016/j.geothermics.2012.10.005.

Witte, H. J. L. (2001), Geothermal response test with heat extraction and heat injection: Examples of application in research and design of geothermal ground heat exchangers, paper presented at the *Europäischer Workshop über Geothermische Response Tests*, Lausanne, Switzerland.

Witte, H. J. L., G. J. van Gelder, and J. D. Spitler (2002), In-situ measurements of ground thermal conductivity: The Dutch perspective, *ASHRAE Trans. Res.*, *108*(1), 263–272.

Woodside, W., and J. H. Messmer (1961), Thermal conductivity of porous media. I. Unconsolidated sands, *J. Appl. Phys.*, *32*(9), 1688–1699.